IMPACT: International Journal of Research in Engineering & Technology
ISSN(P): 2347-4599; ISSN(E): 2321-8843
Vol. 6, Issue 5, May 2018, 49-64

THE INFLUENCE OF HEATING SIDE LENGTH AND CAVITY ORIENTATIONS ON FREE CONVECTION IN A TRAPEZOIDAL ENCLOSURE

Krishne Gowda. B. M[1], M. S. Rajagopal[2], Aswatha[3] & K. N. Seetharamu[4]

[1]Research Scholar, Department of Mechanical Engineering, Sri Krishna Institute of Technology, Bengaluru, India

[2]Research Scholar, Department of Mechanical Engineering, Dayananda Sagara University, Bengaluru, India

[3]Research Scholar, Department of Mechanical Engineering, Bangalore Institute of Technology, Bengaluru, India

[4]Research Scholar, Department of Mechanical Engineering, PES University, Bengaluru, India

Received: 16 May 2018 **Accepted:** 23 May 2018 **Published:** 02 Jun 2018

ABSTRACT

In this paper, a convective heat transfer by laminar free convection in a 2D trapezoidal enclosure is carried out using a control volume based numerical procedure. An enclosure is bounded with parallel heating and adiabatic walls, which are connected by uniformly cooled inclined side walls. A numerical study is carried out using the parameters such as Rayleigh number, Ra ($10^3 \leq Ra\ 10^6$), length of the heating side, ε ($0.4L \leq \varepsilon \leq 0.8L$) and orientation of the cavity, ϕ ($+60^0 \leq \phi \leq -60^0$). The heat transfer and fluid flow are predicted by streamlines, temperature contours, local and overall heat transfer rate. It is seen that heat transfer increases with the increase of Ra, side heating length and angle of orientation of the enclosure. The overall heat transfer rate is a function of cavity angle. On the basis of applications, the heat transfer is controlled by choosing appropriate parameters, the average Nusselt number increases with side length. Maximum heat transfer is found to occur at a horizontal position.

KEYWORDS: *Cavity Orientation, Heat Transfer, Heating Length, Natural Convection, Trapezoidal Cavity*

INTRODUCTION

Natural convection in enclosures has numerous engineering applications which include cooling of electronic components in the cabinet, solar Fresnel reflectors, nuclear reactor cooling, energy efficient rooms and buildings, solar water heating, dynamics of lakes, furnace design, liquid condensers etc. The cooling rate is enhanced by forefront design considerations (McGlen et al., 2004). The free convection in trapezoidal enclosures has been extensively investigated [2-7]. A control volume based numerical work is carried out to predict free convection flow within a partially divided trapezoidal enclosure for two different cases, case1; baffle plates placed vertically on the insulated horizontal bottom wall and case 2; baffles on inclined insulated top wall (Moukalled and Darwish 2003and 2004). The computations are carried out for two different thermal boundary conditions such as left walls, heated by uniform temperature and right side cold wall and vice-versa. The effect of different parameters like *Ra* ranging between 10^3- 10^6, Prandtl number 0.7 to 130, baffle height and location, on the Nusselt number is carried out. It is noted that the Nusselt number decreases in the presence of baffles with different positions and height at the bottom wall. It is noticed that the baffle plate one which is placed closer to the hot wall, decrease the maximum Nusselt number in a trapezoidal enclosure when the height is increased.

The effect of baffle plate on free convection in divergent trapezoidal enclosures with summer day and winter, day boundary conditions has been studied (Arici and Sahin 2009). The computations have been carried out for three types of configurations with different position of the baffle, case 1: no baffle, case 2: the baffle attached to the adiabatic vertical wall and case 3: the baffle at the point of intersection of inclined and vertical walls. It is observed that there is no significant effect of the baffle on the distribution of isotherm contours and Nusselt number during the summer day boundary conditions for Rayleigh number ranges from 10^4 to10^7. However, the Nusselt number is reduced; this is because of the presence of baffle during winter day boundary conditions. It is found that the Nusselt number is high for case1 (without divider) as compared to other two cases (with divider), the heat loss from the cavity is less for case 2 and to obtain the constant temperature distribution within the cavity, the case 3 is ideal. The effect of orientation of the inclined wall on free convection is studied in a trapezoidal enclosure with two vertical baffles mounted on a horizontal surface (Silva et al. 2012). Further, the effect of different angles of inclined wall, *Ra*, *Pr* and divider height on temperature contours, streamlines, local and overall heat transfer rate is numerically investigated by using the finite volume procedure. At higher *Ra* (*Ra* = 10^6), it is seen that the three internal vertices formed due to dividers are combined into a single cell and temperature contours are distorted as the convection currents are more dominant. It is observed that the gradient of temperature and velocity decreases with increase of the baffles height. At fixed dividers height, the overall heat transfer rate increases with the increase of inclined wall angle.

A penalty finite element based method is used to investigate free convection in a trapezoidal enclosure by Natarajan et al. (2008). The bottom wall is heated with constant and sinusoidal variation in temperature. The results are depicted in the form of streamlines, temperature contours, local and average Nusselt numbers for *Ra* ranging from 10^3 to 10^5 and Prandtl number 0.07 to 10. It is noticed that the heating of bottom wall by sinusoidal temperature produces greater heat transfer at the center. However, the average Nusselt number is lower as compared to the constant temperature case and variations in overall heat transfer are more significant for *Pr* ranging between 0.07 to 0.7. The analysis of free convection within a trapezoidal enclosure with the same boundary conditions mentioned earlier and inclined side walls are heated by linearly varied temperature have been carried out by Basak et al. (2009). Also, the computations are carried out for varying the orientation of side wall from 45^0 to 60^0 (trapezoidal cavity) and 90^0 (square cavity). The Nusselt number is found to be higher for a square enclosure than that of trapezoidal enclosure. Dogan et al. (2009) studied numerically heat transfer by convection within the partially opened cavities. The computations have been carried out for different parameters such as position of the opening and its ratios, tilt angles and aspect ratios of the cavity. It is found that the maximum Nusselt number is obtained for tilt angle of 10^0 and an opening ratio of 75% with maximum cavity aspect ratio. A control volume based code is used to study trapezoidal enclosure absorber for a linear Fresnel reflector by Lai et al. (2013). It is reported that the heat loss coefficient is 58% and 47% for insulation and the selective emissivity coating respectively. The glass window can reduce 10.8% utmost cavity depth 150 mm and the ambient temperature effect is small. Manikumar et al. (2015) have been carried out both an experimental and numerical study on plate and tube surface absorbers of a trapezoidal cavity with linear Fresnel reflector solar concentrator system. The trapezoidal enclosure absorber with plot surface is observed to be much better than that of trapezoidal enclosure absorber containing a tube surface.

Recently, Gholizadeh et al. (2016) have carried out a numerical study on double-diffusive free convection within the trapezoidal cavity with an actively heated right side wall. The effect of Grashoff number (10^3 to 10^6), Lewis number

(0.5 to 10), *Pr* (0.7 to 10) and buoyancy ratio (-0.2) for aspect ratio 1 on the overall Nusselt number and Sherwood numbers is studied. It is observed that the Nusselt number and mass transfer increases with raise of Grashoff number. Whereas the mass transfer performance is improving by increase of Lewis number. The natural convection in a trapezoidal enclosure filled with nanoparticles having different conductive obstacles has been carried out (Selimefendigi 2017). The effect of Rayleigh number, orientation of side walls, the fractional volume of nanoparticles, ratio of thermal conductive and shapes of nanoparticles have been investigated. It is found that the Nusselt number increases linearly with increase of fractional volume of nanoparticles. The overall Nusselt number increased in a range between 13% to 16%, with use of cylindrical nanoparticles rather than spherical one. Bondareva et al. (2018) have studied the transient natural convection in a trapezoidal cavity. The influence of water-based nanofluids, openings, thermophoresis and Brownian diffusion effects on transient natural convection is studied. It is reported that the average Nusselt number at inclined heating wall rises with the increase of *Ra* and it is decreasing with increase of other parameters.

As seen from the literature, the most of numerical studies deal with the free convection in cavities of simple geometries like square, rectangular, cylindrical shapes, etc. However, the study on natural convection within the trapezoidal enclosures is limited to temperature boundary conditions only. It is found from the literature that no attempt has been made to study the influence of different lengths of heating side and angle of orientations of the trapezoidal cavity on natural convection. Therefore it is interesting to persue the complete understanding the thermal performances of the trapezoidal cavity with linear Fresnel reflectors, the enclosures of LED (Light Emitting Diode) lighting system, the lowest power consumption buildings and room's design for their cooling etc. Thus, the main objective of present study is to predict the influence of the different lengths of heated bottom wall, orientations of cavity, and Rayleigh number on flow of fluid and average Nusselt number within a trapezoidal cavity.

HEAT TRANSFER MODEL

Physical Model

The physical model of a computational domain is a 2D trapezoidal cavity with inclined side walls of height H, top wall of length L and hot bottom wall as shown in Figure1. The varying bottom wall is heating at constant temperature (T_h), sloping cold walls are subjected to uniform temperature (T_c) and insulated the top wall. The computations have been investigated for **ε** = 0.4L and 0.8L and cavity angle ϕ = + 60^0 to - 60^0.

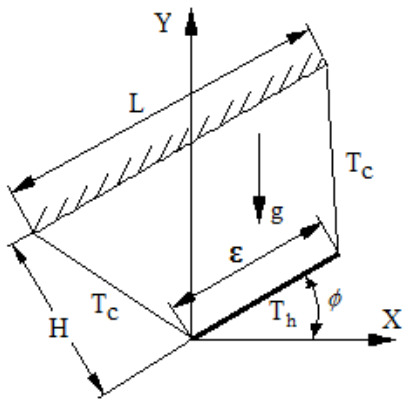

Figure 1: Physical System of a Computational Domain

Mathematical Models and Boundary Conditions

The flow of fluid within the cavity is assumed to be Newtonian, incompressible and laminar. The no-slip boundary conditions are considered for all walls. There are no internal heat generations and thermal radiative transfer of heat. The buoyancy terms are invoked by Boussinesq approximation to couple temperature and flow field. Based on these assumptions and descriptions, the equations governing laminar free convection flow using conservations of mass, momentum and energy in dimensional form are given below:

$$\frac{\partial U}{\partial X}+\frac{\partial V}{\partial Y}=0 \tag{1}$$

$$U\frac{\partial U}{\partial X}+V\frac{\partial U}{\partial Y}=-\frac{\partial P}{\partial X}+\Pr\left(\frac{\partial^2 U}{\partial X^2}+\frac{\partial^2 U}{\partial Y^2}\right) \tag{2}$$

$$U\frac{\partial V}{\partial X}+V\frac{\partial V}{\partial Y}=-\frac{\partial P}{\partial Y}+\Pr\left(\frac{\partial^2 V}{\partial X^2}+\frac{\partial^2 V}{\partial Y^2}\right)+Ra\,\Pr\,\theta \tag{3}$$

$$U\frac{\partial \theta}{\partial X}+V\frac{\partial \theta}{\partial Y}=\frac{\partial^2 \theta}{\partial X^2}+\frac{\partial^2 \theta}{\partial Y^2} \tag{4}$$

The following are the transformation of variables used to write non-dimensional form of governing equations.

$$X=\frac{x}{H},Y=\frac{y}{H},U=\frac{uH}{\alpha},V=\frac{vH}{\alpha},\theta=\frac{T-T_c}{T_h-T_c}$$
$$P=\frac{pH^2}{\rho\alpha^2},\Pr=\frac{\nu}{\alpha},Ra=\frac{g\beta(T_h-T_c)L^3\,\Pr}{\nu^2} \tag{5}$$

The control volume based method [20] built in ANSYS CFD software [21] is used to solve the governing equations (2) to (5) for boundary conditions mention below. The physical domain is discretized into a finite number of control volumes (or cells) and integrates the governing equations over each control volume. Therefore the solution domain is discretized (meshed) by dividing it into quadrilateral cells.

The boundary conditions for physical domain given in figure1are specified as follows;

Top wall; $U=V=0,\ \frac{\partial\theta}{\partial Y}=0$

Bottom hot wall: $U=V=0,\ T=T_h$ **(6)**

Right and left cold walls: $U=V=0, T=T_C$

EVALUATION OF STREAMFUNCTION AND NUSSELT NUMBER

Stream Function

The stream functions in fluid flow problems are used to display the motion of the fluid which are obtained from the velocity fields U and V in X and Y directions respectively. Bachelor [22] dealt the relationship between the streamlines

ψ and velocity components for 2D flows and is given below;

$$U = \frac{\partial \psi}{\partial Y} \text{ and } V = -\frac{\partial \psi}{\partial X} \quad \textbf{(7)}$$

The single equation is of the form: $\frac{\partial^2 \psi}{\partial X^2} + \frac{\partial^2 \psi}{\partial Y^2} = \frac{\partial U}{\partial Y} - \frac{\partial V}{\partial X}$ **(8)**

Local and Average Nusselt Numbers

The gradients of heat transfer is defined in terms of local Nusselt number,

$$Nu = -\frac{\partial \theta}{\partial n} \quad \textbf{(9)}$$

Where, 'n' is direction to a plane. The average Nusselt numbers for the non-dimensional heating length of bottom wall are obtained by;

$$\overline{Nu_b} = \frac{1}{\varepsilon}\int_0^{\varepsilon} Nu_b dX \quad \textbf{(10)}$$

The integrations of the above equations are performed using the trapezoidal rule.

Numerical Technique

The physical domain considered for numerical study is discretized into a finite number of volumes. In this study, the governing equations are integrated over the control volume to obtain a set of algebraic expressions. The solution method is using the least squares cell-based gradient evaluation for the spatial discretization, where linearly varied dependent variables are assumed between the cell centers [20]. The central differencing scheme is used to approximate the diffusion terms of energy and momentum equations. The convection-diffusion terms formulation of momentum and energy equations are obtained by using the second order upwind scheme. PISO (*P*ressure-*I*mplicit with *S*plitting of *O*perators) method developed by Issa [23] is used to solve discretized equations. The iterative solution and the under relaxation factors of 0.3, 0.7 and 1.0 are used for solving the pressure, momentum, and energy equations, respectively. The residuals presented in the governing equations are based for convergence criterion. The iterations are stopped, when all the residuals are converged to 10^{-5}.

Numerical Resolution

The physical domain of trapezoidal cavity is meshed with four noded rectangular cells. To predict the computation accuracy of the present code, the free convection flow of fluid in a trapezoidal enclosure with bottom wall heating by Natarajan et al. [12] is considered for the analysis. Computations are carried out using a Galerkin finite element method for *Ra* ranging from 10^3 - 10^5, *Pr* = 0.07 - 10. The suitable grid size is selected by carrying the computations for *Ra* = 10^5, *Pr* = 0.7. The orientations of uniformly cooled side walls are $\varphi = 30^0$ with vertical. Grid generation is carried out using Gambit software. The present study is carried out for various grid sizes ranging from 21 x 21to 81 x 81for a step of 10 elements presented in table 1. The comparison of present $\overline{Nu}$ with that of Natarajan et al. [12] at Ra = 10^5. It is seen that

the $\overline{Nu}$ for 21 x 21 is about 7.32 and it increases as the grid is refined and reaches almost a constant value of 7.86 for a grid size of 61 x 61. This value remains sensibly constant for grid of sizes 71 x 71 and 81 x 81. Hence, for further calculations a grid of 61 x 61 is considered. Further, the comparison of the average Nusselt number for different Rayleigh number is presented in Table 2. It is observed from the table 2 that there is good agreement between Natarajan et al. [12] and present study with the maximum discrepancy of less than 1.0 %.

Table 1: Grid Independence Study Results with $Ra = 10^5$

Grid size	$\overline{Nu}$ [Present]	$\overline{Nu}$ [12]
21 x 21	7.32	7.85
31 x 31	7.35	
41 x 41	7.51	
51 x 51	7.72	
61 x 61	7.86	
71 x 71	7.85	
81 x 81	7.86	

Table 2: Comparison of $\overline{Nu}$ with the Values of [12] for Full Length Heated of Bottom Wall

$\overline{Nu}$	*Ra*		
	10^3	10^4	10^5
Natarajan et al. [12]	4.19	5.35	7.85
Present study	4.22	5.35	7.86

RESULTS AND DISCUSSIONS

Effect of *Ra*: Constant Temperature at Bottom Wall

The contours of streamlines and isotherm have been compared with Gaussian quadrature based finite element procedure [12] and are in good agreement. In the present study, a finite volume method gave smooth solutions at interior points and corners of the domain. The fluid flow field of the enclosure is displayed in form of streamlines and temperature as isotherm contours.

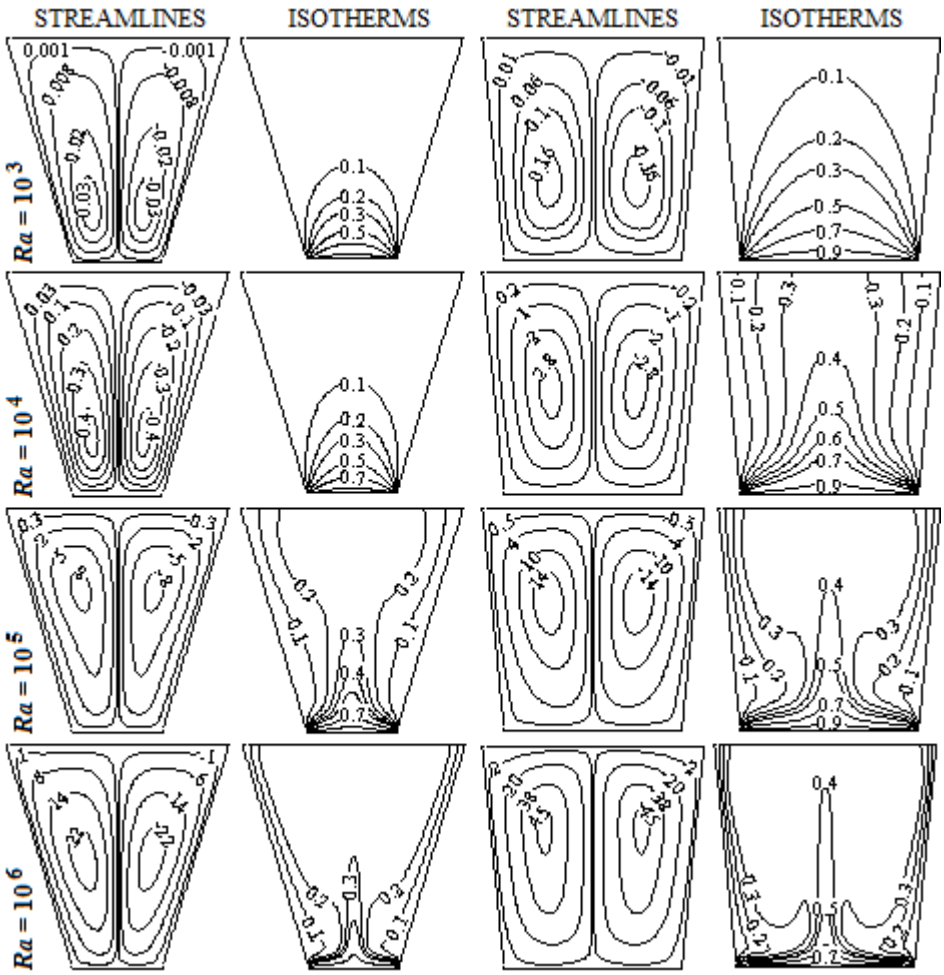

(a) $\varepsilon = 0.4L$ (b) $\varepsilon = 0.8L$

Figure 2: Streamlines and Isotherm Contours for Various *Ra*

Figure 2 shows the streamlines and isotherm contours for ε = 0.4L and ε = 0.8L of heating bottom wall for Rayleigh number ranges from 10^3 to 10^6 at $\phi = 0^0$. Owing to cooling of enclosure symmetrically on the inclined side walls, the streamlines and isotherm contours are symmetrical about the vertical centre line. The vertical symmetric boundary conditions results a two re-circulating cells, one in the left halve and another in the right halve of the trapezoidal cavity for values of the *Ra* considered. Therefore, the magnitude of the streamlines in the both left and right half of the enclosure about vertical symmetry is identical but the sense of rotation is different. As the fluid rises from the middle of the horizontal bottom hot wall, the cells ascend with the vertical symmetry line, then strikes the top adiabatic wall through which it flows horizontally towards the respective cold vertical walls and it flows down along the side cold walls as it cools down. As predicted, due to symmetrically cooled inclined walls, the fluid flow rising from central part of the bottom heating wall and flows down the inclined wall caused by top adiabatic wall two similar cells with clockwise and counter-clockwise circulations within the cavity. It is observed from figure 2 that the shape of the bifurcated streamline contours inside the enclosure is similar to that of the cavity.

Figure 2(a) shows the streamlines and temperature contours for different Rayleigh number. At *Ra* = 10^3, the

magnitude of the streamlines are very low (ie., ψ = 0.001 - 0.03) because of the conduction dominated heat transfer within the enclosure. In the conduction dominating state, there is no significant variation in isotherm contours with respect to *Ra* and the significant convection currents may be initiated closer to $Ra = 10^4$. The magnitudes of circulations are greater nearer to hot walls or middle of the enclosure, this is because of no-slip boundaries at all walls of the cavity. The eyes of the both cells are concentrating nearer to hot bottom wall. The isotherm contours are smooth curves near the heating wall and symmetric with the vertical center line. As the *Ra* increases to 10^4, the values of streamlines start increasing to 0.4 and isotherm contours are raising. The isotherm contour one which at top (θ = 0.1) reaches to middle of the cavity. As *Ra* increases to 10^5 the convection currents caused by buoyancy forces increases to a greater magnitude (seen in figure 2(a)). As magnitudes of circulations rises with an increase of Rayleigh number, the isotherms are compressed nearer to cold walls just above the top half of the cavity only. As a result, the nucleus of circulations is settled just above the center half of the enclosure. There is significant development in the formation of the thermal boundary layer adjacent to vertical cold and bottom hot wall. At $Ra = 10^6$, the convection currents dominating more than at $Ra = 10^5$. Due to greater convection currents, the compression of the isotherm contours increased further inside the cavity in the downward direction and it reaches almost 95% of the height of the cavity. The gradients in temperature are smaller in isotherms and higher stratification zones of isotherm contours is seen at vertical line (symmetry) because of fluid flow is stagnant near the walls. Therefore, the thermal boundary layer becomes thinner and spreads through the inclined hot and cold walls of the cavity.

Effect of Rayleigh Numbers: Different Lengths of Hot Bottom Wall

Comparative study between figures 2(a) and (b) shown that as 'ε' increases from 0.4L to 0.8L, the magnitude of the central core of streamlines are increasing and isotherms are raising within the cavity to a greater extent. As 'ε' increases from 0.4L to 0.8L, the central core of streamlines is bigger in size, due to the larger distance between cold walls. Consequently, at $Ra = 10^5$ and 10^6, the values of the streamlines is almost double and the core of streamlines is placed just above the midpoint of the vertical symmetry, signifying the enhancement in the intensity of circulations for ε = 0.8L than that of ε = 0.4L. In addition, at higher Rayleigh numbers ($Ra = 10^5$ and 10^6), the isotherm contours ($\theta \leq 0.3$) are moving nearer to the inclined cold walls and still continuously and this is more for ε = 0.4L. For higher Ra and ε = 0.4L, the isotherm contour $\theta \geq 0.3$ is symmetric about a vertical symmetric line and it spreads the entire span of heating wall. The order of isotherms at the vertical line of symmetry decreases, further to $\theta \geq 0.4$. For ε = 0.4, the thermal boundary layer formation near the cold walls and hot wall is thinner than that of ε = 0.3due to the significant increase of the Nusselt number with increase in heating length ε.

Effect of Rayleigh Numbers: Cavity Angles

The streamlines and isotherm contours for various cavity angles at Rayleigh number $Ra = 10^5$ is depicted in figure 3. The effect of cavity orientation for a step angle of 30^0 in clockwise (negative sign) and anti-clockwise (positive sign) direction from the horizontal position ($\phi = 0^0$) of the bottom heating wall is studied.

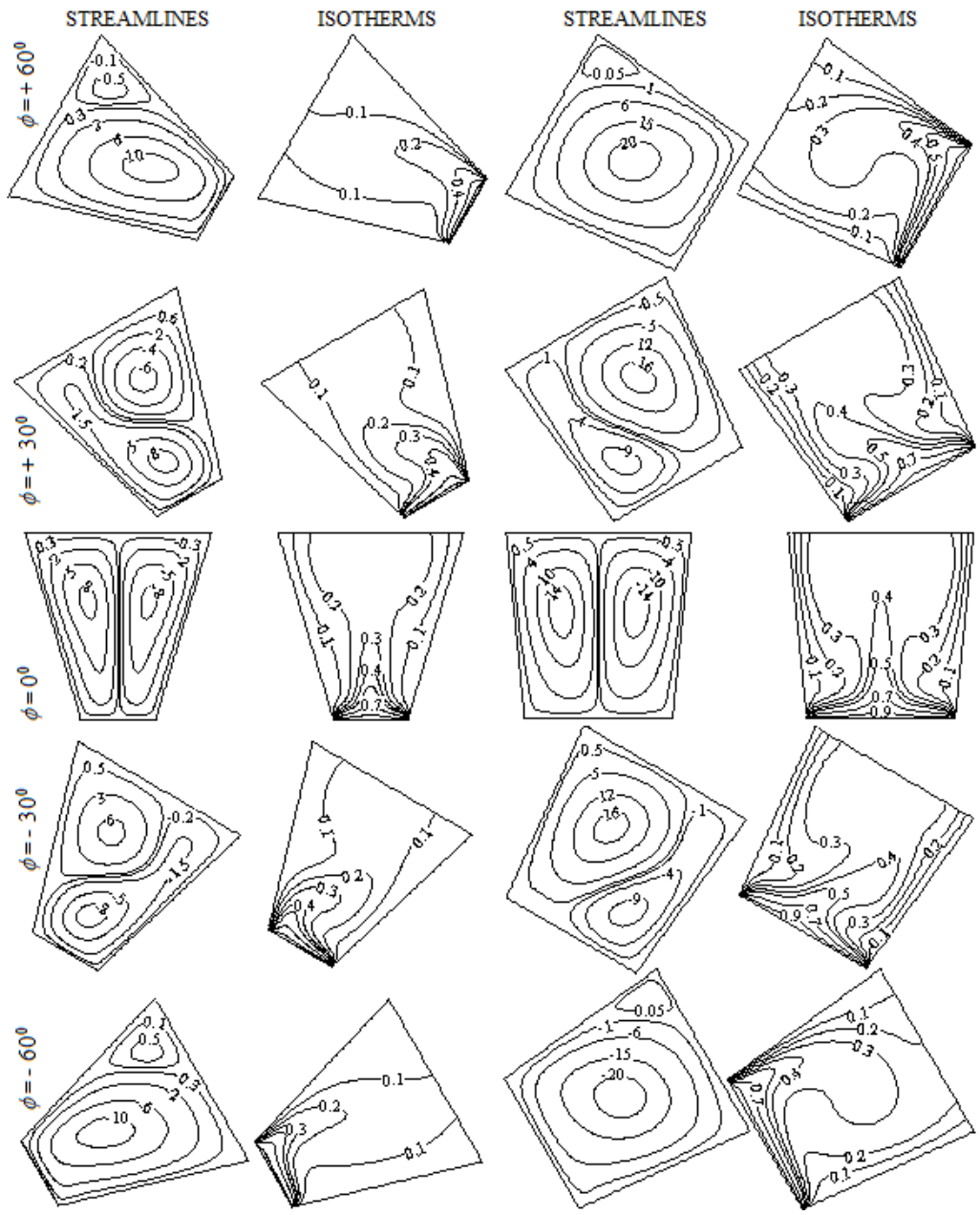

(a) $\varepsilon = 0.4L$ (b) $\varepsilon = 0.8L$

Figure 3: Streamlines and Isotherm Contours for Different Orientations of the Cavity at *Ra* = 10^5

The streamlines and isotherm for heating side length $\varepsilon = 0.4L$ at *Ra* = 10^5 is shown in figure 3(a). At $\phi = 0^0$, the fluid is raising from the center of heated bottom wall and it is bifurcated at the top insulated wall forming two symmetrical cells of the same magnitude. Moreover, for an inclined enclosure this symmetry is destroyed completely as the buoyancy force starts acting both in x- and y-directions. When the cavity is revolving either in the clockwise or counter-clockwise direction, the fluid moves vertically upward direction. The maximum heat is transferred, when the fluid moving along the nearest top cold wall. The flow is retarded in the top as it moves upward direction, presumably due to not easy path for turning in a sharp corner. However, the cavity angle $\phi \leq 45^0$ the stagnation area of fluid flow is increasing and it decreases

with increase of cavity angle till it reaches 90^0. As the cavity starts rotating clockwise direction from the horizontal position, the right cell starts moving towards the top sharp corner and extending downward direction. Consequently, the lower vertex gets distorting from hot wall to opposite adiabatic wall along with lower cold wall with highest magnitude. The isotherm contours are also altered in accordance with the flow fields and moves towards the top cold walls as shown in figure 3 for both (ϕ = 30^0 and 60^0) cavity angles. It is observed from the figure 3(a) that the vertices exhibit similar behavior irrespective of the sense of rotation of the enclosure. Also, it is noticed that the overall magnitude of streamlines to horizontal (ϕ = 0^0) heating bottom wall is higher than that of the other two angles (ϕ = 30^0 and 60^0) considered for the study.

Figure 3(b) illustrates, the streamlines and isotherm contours for heating side length $\varepsilon = 0.8L$ for cavity angles ϕ = 0^0, ϕ= 30^0 and ϕ= 60^0. It is evident that the similar behavior is observed for both streamlines and isotherm contours that of $\varepsilon = 0.4L$. However, the magnitude of the vertices increases with increase of heating side length. At $\varepsilon = 0.4L$ with horizontal bottom heating wall, the two lowest isotherm contour (θ = 0.1 and 0.2) are opened at the top and this has been reduced to θ = 0.1 for another two cavity angles considered for the study. This is enhanced to θ = 0.3 at angles ϕ= 0^0, ϕ= 30^0 and reduced to θ = 0.2 at ϕ= 60^0 for side heating length $\varepsilon = 0.8L$.

Rate of Heat Transfer: Local and Average Nusselt Numbers

Figure 4 and 5 display the effect of the Rayleigh number on local heat transfer for both horizontal bottom hot and right side cold walls at $\varepsilon = 0.8L$. The variations of local Nusselt number along with the bottom hot wall are depicted in figure 4(a) and are symmetric about lines of symmetry due to similar (symmetric) boundary conditions. It is found that the local heat transfer at 10% on either side of the bottom wall and 15% at the beginning and end of the bottom hot wall remains unchanged for *Ra* = 10^3 and 10^4. The initiation of the convection may take place at *Ra* $\geq$ 5 x 10^3. Further, the local heat transfer is increasing with the increase of *Ra* as a significant convection mode heat transfer is dominating. The isotherm contours are compressed from corners of the cavity towards the vertical center line and values of the streamlines are increasing. The rate of heat transfer is lower at the center of the cavity due to a larger distance from cold walls.

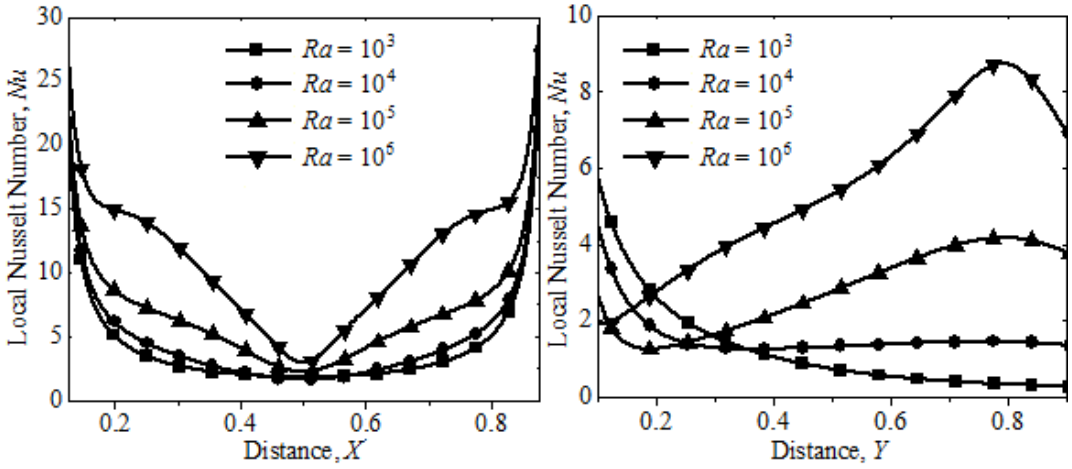

(a) Bottom Hot Wall, ε = 0.8L and ϕ = 0^0 **(b) Right Side Cold Wall, ε = 0.8L and ϕ = 0^0**

Figure 4: Variations of *Nu* for Different *Ra*

The variation of Nu at different Ra along with the right side cold wall is illustrated in figure 4(b). As evident of conduction dominated heat transfer at $Ra = 10^3$, the *Nu* decreases monotonically along the cold side wall. At higher *Ra*, it is observed that the *Nu* at the beginning is decreasing, increasing and again decreasing. This is because of the temperature contours are largely compressed near the central part of the side cold wall, due to stronger recirculation and lesser thermal gradients. The heat transfer decreases in trend at the corners because of flow is retarded as it takes turns. In addition isotherm contours are deformed towards, side walls, away from top corners formed by adiabatic top wall and discontinuities at bottom corners due to heating of bottom wall by constant temperature. The local Nusselt numbers are similar in trend but it decreases with decreasing in ε .

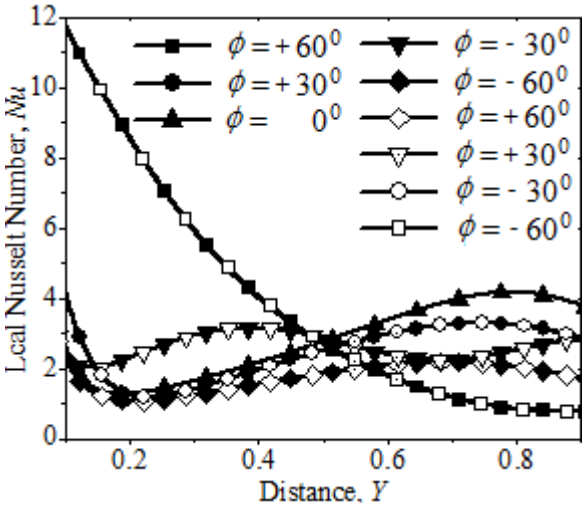

Figure 5: Variations of *Nu* for Right Side Cold Wall (Filled), Left (un-filled) $\mathcal{E}$ = 0.8L and *Ra* = 10^5

Figure 5 depicts the variation in *Nu* with distance for different cavity angle at Ra = 10^5 and $\mathcal{E}$ = 0.8L The streamline and isotherm contours have similar trends when the cavity rotates in clockwise direction about left corner and anti-clockwise direction about right corner or with respect to centre of bottom wall. As the cavity rotates in anti-clockwise (-ve) direction about left bottom cornwr, cold wall at the right side moves to top and left cold wall is at the bottom and it is vice-versa in the clockwise (+ve) direction. It is intresting to find from the figure 5 that the local heat tranfer is of similar trend for left or right side cold walls irrespective of the sense of rotations of the cavity. Therfore, the authors considered the variations of parameters in anti-clock wise directions for further analysis.. The variations in *Nu* for a sense of rotations of heating wall has not been dealt, due to fact that the trends are identical.

The distribution of average Nusselt number at hot and cold side walls versus Rayleigh numbers is illustrated in figures 6 and 7. Figure 6 shows the variations of $\overline{Nu}$ and logarithmic *Ra* for $\varepsilon = 0.4L$ and 0.8L at bottom heating wall for cavity angle ϕ = 0^0, 30^0 and 60^0. It is found that the $\overline{Nu}$ is high at all the points for $\varepsilon = 0.8L$ as compared to $\varepsilon = 0.4L$. It is noted that the magnitude of $\overline{Nu}$ for $\varepsilon = 0.8L$ is more compared to $\varepsilon = 0.4L$. This is because the amount of heat supplied increases with increase of 'ε' for temperature boundary conditions. At higher *Ra*, the values of the streamlines of $\varepsilon = 0.8L$ are higher as compared to $\varepsilon = 0.4L$. For $\varepsilon = 0.4L$, lower values ($\theta \leq 0.2$) of the isotherm contours is opened and compressed towards the cold walls at horizontal position of heating wall. Further, it is reduced to θ = 0.1for ϕ = 30^0 and

60^0, signifing that the heat transfer reduces with any cavity angle other than horizontal position. Therefore, the $\overline{Nu}$ is higher at horizontal position compared to any other inclination of the cavity.

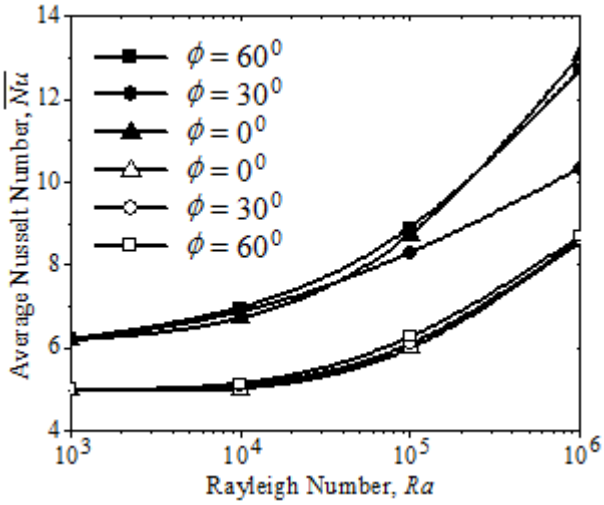

Figure 6: Variations of $\overline{Nu}$ for Bottom Hot Wall; ε = 0.8L (Filled) and ε = 0.4L (Un-filled)

At higher *Ra*yleigh numbers ($Ra \geq 10^4$), it is observed from the figure 2 that the top opening of isotherm contours for $\varepsilon = 0.8L$ is greater ($\theta \leq 0.2$) than that of $\varepsilon = 0.4L$. Consequently, the $\overline{Nu}$ increases with increase of length of heating side. From the log-log plot of $\overline{Nu}$ versus *Ra* (not shown), it is found that heat transfer by conduction is dominant for $\varepsilon = 0.4L$ at $Ra < 10^4$. However, this is reduced to $Ra \leq 5 \times 10^3$ for $\varepsilon = 0.8L$.

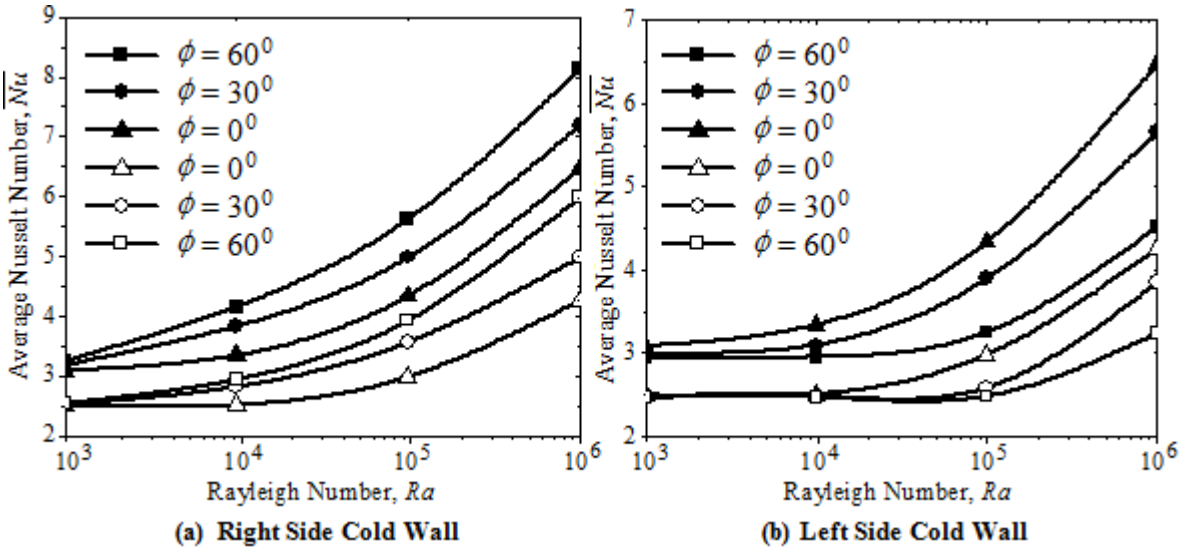

Figure 7: Variations of $\overline{Nu}$ Versus *Ra* for Side Walls

Figures 7(a) and (b) depicts the variation of $\overline{Nu}$ versus logarithmic values of *Ra* for right and left cold walls at different cavity angles. The cavity is rotating in anti-clockwise direction about left bottom corner for a step of 30^0 from the horizontal position of the bottom heating wall. The fluid rises from vertically from the heating wall and maximum heat is

transferred to the top side cold wall as it moves along. Consequently, the isotherm contours follow the fluid flow and it extends parallel to top cold wall. As the angle of the orientation is increased, the right top cell moves towards the top corner. The magnitude and size of the streamlines placed at below is increased with increase of ϕ and has extend it to cold wall. On the contrary, the magnitude is decreasing and size becomes smaller and smaller. Therefore, it has noted from the figure 7 that the $\overline{Nu}$ rising with an increase of 'ε/ at all the points along the side walls. At the top side (right) cold, the $\overline{Nu}$ increases and it decreases in bottom side of the cold wall with an increase of cavity angle 'ϕ'.

Table 3: Power Law Correlations Between $\overline{Nu}$ and *Ra* for both Bottom Hot and Side Cold Walls

ε	ϕ	Bottom Heating Wall		Right Side Cold Wall	
		Corrolation	R^2	Corrolation	R^2
0.8L	60^0	$\overline{Nu} = 2.476Ra^{0.113}$	0.997	$\overline{Nu} = 1.134Ra^{0.141}$	0.997
	30^0	$\overline{Nu} = 1.155Ra^{0.131}$	0.998	$\overline{Nu} = 1.155Ra^{0.131}$	0.998
	0^0	$\overline{Nu} = 2.164Ra^{0.124}$	0.995	$\overline{Nu} = 0.977Ra^{0.135}$	0.998
0.4L	0^0	$\overline{Nu} = 0.930Ra^{0.108}$	0.998	$\overline{Nu} = 0.930Ra^{0.108}$	0.998
	30^0	$\overline{Nu} = 2.037Ra^{0.099}$	0.996	$\overline{Nu} = 0.940Ra^{0.119}$	0.998
	60^0	$\overline{Nu} = 0.856Ra^{0.137}$	0.998	$\overline{Nu} = 0.856Ra^{0.137}$	0.998

The log-log plot is drawn and data is collected for more than 50 points. The power law correlations are obtained and presented in the Table 3 for both hot bottom and right side cold walls of the trapezoidal cavity. The convection is initiated, from $Ra \geq 10^4$ for $\varepsilon = 0.4L$ and whereas it is from Ra ≥ 5 x 10^3 for $\varepsilon = 0.8L$.

CONCLUSIONS

In the present study the influence of length of heating wall, cavity angle and the characteristics of heat transfer on free convection within the trapezoidal cavity has been investigated in detail. The finite volume based computational procedure is used to get smooth solutions in the form of streamlines and temperature contours when bottom wall is subjected to uniform temperature with various cavity angles and Rayleigh numbers. The following observations are made during the present investigations:

- For $\varepsilon = 0.4L$, the heat transfer by conduction dominating mode is observed for $Ra \geq 10^4$ and whereas, it reduces to $Ra \geq 5$ x 10^3 for $\varepsilon = 0.8L$.
- In the convection dominating mode of heat transfer, $\overline{Nu}$ monotonically increases with increase of the Rayleigh number for both heating and cold side walls irrespective of length of heating wall.
- The overall rate heat transfer increases with increase of Rayleigh number and length of heating wall.
- At higher *Ra*, the size and values of the upper cell decreases due to domination and extends along the upper cold walls of lower cell as the cavity angle increases.
- Highest Nusselt number is obtained, when heating wall is at horizontal ($\phi = 0^0$) position compared to other different cavity angles due to symmetric boundary conditions.

- Due to symmetric boundary conditions, the magnitude and shapes of streamlines are identical for the same angle of rotation of the cavity irrespective of sense of rotation.
- It is dealt in the literature that the detailed computations of local and overall heat transfer rates on a free convection within a trapezoidal enclosure for various cavity inclinations and heating length of bottom wall have not been studied.
- It is very important to show free convection within the cavity, to pursue for a complete knowledge of average Nusselt number for many science and engineering systems such as design of solar Fresnel reflectors, solar water heating systems, cooling of electronic components, cooling of nuclear reactors, energy efficient rooms and buildings etc.

REFERENCES

1. *R. J. McGlen, R. Jachuk, and S. Lin, Integrated thermal management techniques for high power electronic devices, Applied Thermal Engineering, 24, 2004, 1143-1156.*
2. *E. Natarajan, S. Roy, S, and T. Basak, Effect of various thermal boundary conditions on natural convection in a trapezoidal cavity with linearly heated side wall(s). Numer. Heat Transf. Part B, 52, 2007, 551–568.*
3. *F. Moukalled, and M. Darwish, Natural convection in a partitioned trapezoidal cavity heated from the side. Numer. Heat Transf. Part A, 43, 2003, 543–563.*
4. *T. Basak, S. Roy, and I. Pop, Heat flow analysis for natural convection within trapezoidal enclosures based on heatline concept. Int. J. Heat Mass Transf. 52, 2009, 2471–2483.*
5. *E. Fontana, A. da Silva, V. C. Mariani, and F. Marcondes, The influence of baffles on the natural convection in trapezoidal cavities. Numer. Heat Transf. Part A, 58, 2010, 125–145.*
6. *M. Bhattacharya, T. Basak, H. F. Öztop, and Y. Varol, Mixed convection and role of multiple solutions in lid-driven trapezoidal enclosures. Int. J. Heat Mass Transf. 63, 2013, 366–388.*
7. *M. M. Gholizadeh, N. Rasoul, K. Javad, and A. Ghasemi, Numerical study of double diffusive buoyancy forces*
8. *induced natural convection in a trapezoidal enclosure partially heated from the right sidewall, Alexandria Engg. Journal, 55, 2016, 779-795.*
9. *F. Moukalled, and M. Darwish, Natural convection in a partitioned trapezoidal cavity heated from the side, Numer. Heat Transfer A 43, 2003, 543-563.*
10. *Muhammad Sajjad Hossain & Mohammad Abdul Alim, Effects of Heat Flow Patterns for MHD Free Convection within Trapezoidal Cavity Based on Heatline Concept, International Journal of Mathematics and Computer Applications Research (IJMCAR), Volume 3, Issue 2, May-June 2013, pp. 87-102*
11. *F. Moukalled, and M. Darwish, Natural convection in a trapezoidal enclosure heated from the left side with baffle*

mounted on its upper inclined surface, Heat Transfer Eng. 25, 2004, 80-93.

12. *M. E. Arici and B. Sahin, Natural convection heats transfer in a partially divided trapezoidal enclosure, Therm. Sci. 13, 2009, 213-220.*
13. *A. Silva, E. Fontana, V. C. Mariani, and F. Marcondes, Numerical investigation of several physical and geometric parameters in the natural convection in to trapezoidal cavities, Int. J. of Heat Mass Transfer, 55, 2012, 6808-6818.*
14. *E. Natarajan, T. Basak, and S. Roy, Natural convection flows in a trapezoidal enclosure with uniform and non-uniform heating of bottom wall, Int. J. of Heat and Mass Transfer, 51, 2008, 747-756.*
15. *T. Basak, S. Roy, A. Singh, and B.D. Pandey, Natural convection flow simulation for various angles in a trapezoidal enclosure with linearly heated side wall(s), Int. J. Heat Mass Transfer, 52, 2009, 4413-4425.*
16. *A. Dogan, S. Baysal, and S. Baskaya, Numerical analysis of natural convection heat transfer from partially open cavities heated from one wall, J. of Thermal Sci. and Technology, 29(1), 2009, 79-90.*
17. *Y. Lai, T. Wu, S. Che, Z. Dong, and M. Lyu, Thermal performance prediction of a trapezoidal cavity absorber for a linear Fresnel reflector, Advance in Mechanical Engineering, 2013, 1-7.*
18. *R. Manikumar, R. Palanichamy, and A. V. Arasu, Heat transfer analysis of an elevated linear absorber with trapezoidal cavity in the linear Fresnel reflector solar concentrator system, J. Thermal Sci., 24, 2015, 90-98.*
19. *M. M. Gholizadeh, R. Nikbakhti, J. Khodakhah, and A. Ghasemi, Numerical study of double diffusive buoyancy forces induced natural convection in a trapezoidal enclosure partially heated from the right side wall, Alexandria Engineering Journal, 55, 2016, 779-795.*
20. *F. Selimefendigil, Natural convection in a trapezoidal cavity with an inner conductive object of different shapes and filled with nanofluids of different nanoparticle shapes, Iran J Sci. Technology, Trans. Mech. Eng. 2017, 1-16.*
21. *N. S. Bondareva, M. Sheremet, H. F. Öztop, N. Abu-Hamdeh, Transient natural convection in a partially open trapezoidal cavity filled with a water-based nanofluid under the effects of Brownian diffusion and thermophoresis, Int. J. of Numerical Methods for Heat & Fluid Flow, 28(3), 2018, 606-623.*
22. *S. V. Patankar, Numerical Heat Transfer and Fluid Flow. McGraw-Hill, New York, 1980.*
23. *ANSYS FLUENT User's Guide, ANSYS, Inc., Southpointe 275, Technology Drive Canonsburg, PA, 15317, 2011.*
24. *G. K. Batchelor, An introduction to fluid dynamics. Cambridge University Press, 1993.*
25. *R. I. Issa, Solution of the implicitly discretized fluid flow equations by operator splitting, J. Coput. Phys., 62, 1985, 40-65,*

APPENDICES

Table 4

Nomenclature			
	heat capacity, J/kg K	x, y	Cartesian coordinates
	acceleration due to gravity, m/ s^2	***Greek Symbols***	
	cavity height, m	α	thermal diffusivity, m^2/s
	thermal conductivity, W/ m K	β	volume coefficient of thermal expansion, 1/K
	cavity width, m	ν	kinematic viscosity, m^2/ s
	local Nusselt number	ρ	fluid density, kg/ m^3
	pressure, Pa	ψ	stream function
	dimensionless pressure, $(p-p_\infty)B^2/\rho\alpha^2$	θ	dimensionless temperature, $(T-T_\infty)/(T_h-T_\infty)$
	Prandtl number, ν/α	ϕ	inclination angle of the heated wall from the horizontal, ^{o}
	regression coefficient	*Superscripts*	
	Rayleigh number, $g\beta\Delta TL^3/(\nu\alpha)$	$\bar{}$	average
	temperature difference, T_h-T_∞	*Subscripts*	
	temperature, K	c	cold
	dimensionless fluid velocities, uL/α, vL/α	h	hot
	ionless volume flow rate through the opening, $\int_{x=1} U_{in}\,dY$	∞	ambient value
X, Y	dimensionless cartesian coordinates, *x/L, y/L*		